



HAL
open science

Atmospheric Fate and Impact of Perfluorinated Butanone and Pentanone

Yangang Ren, François Bernard, Véronique Daële, Abdelwahid S Mellouki

► **To cite this version:**

Yangang Ren, François Bernard, Véronique Daële, Abdelwahid S Mellouki. Atmospheric Fate and Impact of Perfluorinated Butanone and Pentanone. *Environmental Science and Technology*, 2019, 53 (15), pp.8862-8871. 10.1021/acs.est.9b02974 . insu-02262364

HAL Id: insu-02262364

<https://insu.hal.science/insu-02262364>

Submitted on 2 Aug 2019

HAL is a multi-disciplinary open access archive for the deposit and dissemination of scientific research documents, whether they are published or not. The documents may come from teaching and research institutions in France or abroad, or from public or private research centers.

L'archive ouverte pluridisciplinaire **HAL**, est destinée au dépôt et à la diffusion de documents scientifiques de niveau recherche, publiés ou non, émanant des établissements d'enseignement et de recherche français ou étrangers, des laboratoires publics ou privés.

1 **Atmospheric fate and impact of perfluorinated**
2 **butanone and pentanone**

3
4 Yangang Ren, François Bernard, Véronique Daële, Abdelwahid Mellouki*

5
6
7 **Affiliations**

8 Institut de Combustion Aérothermique, Réactivité et Environnement, Centre National
9 de la Recherche Scientifique (ICARE-CNRS), Observatoire des Sciences de l'Univers
10 en région Centre (OSUC), CS 50060, 45071 cedex02, Orléans, France

11
12 **Corresponding author**

13 * mellouki@cnrs-orleans.fr

14
15
16 **Journal:** Environmental Science and Technology

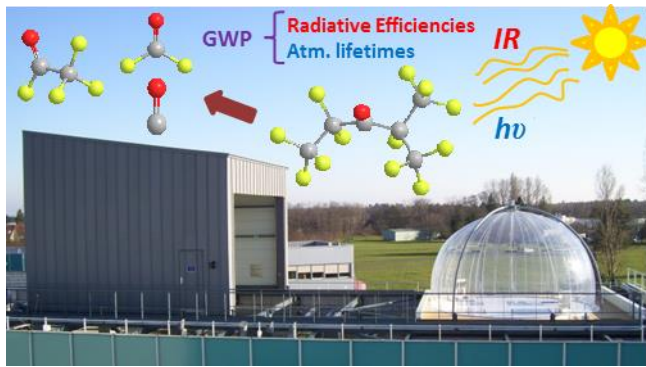
17

18 **Abstract**

19 Perfluoroketones, used as replacement to halons and CFCs, are excluded from the
20 Montreal Protocol because they are considered as non-ozone depleting substances.
21 However, their chemical structure makes them possible greenhouse gases if their
22 atmospheric lifetimes are long enough. To assess that possibility, we investigated the
23 photolysis of perfluoro-2-methyl-3-pentanone (PF-2M3P), and perfluoro-3-methyl-2-
24 butanone (PF-3M2B) using outdoor atmospheric simulation chambers. In addition, the
25 photolysis of a non fluorinated pentanone (2-methyl-3-pentanone, 2M3P) was studied.
26 The results showed that photolysis is the dominant loss pathway of PF-2M3P and PF-
27 3M2B in the troposphere whereas 2M3P is lost by both photolysis and gas phase
28 reaction with atmospheric oxidants. The photolysis effective quantum yields of PF-
29 2M3P, PF-3M2B and 2M3P were estimated and some of the main products identified.
30 The photolysis of PF-2M3P and PF-3M2B was found to have a minor impact on the
31 atmospheric burden of fluorinated acids. The atmospheric lifetimes of PF-2M3P, PF-
32 3M2B and 2M3P were estimated to 3-11 days, ~13 days and 1-2 days, respectively.
33 Combining the obtained data, it has been concluded that with 100-year time horizon
34 global warming potentials (GWP₁₀₀) equivalent to <0.21, ~0.29 and $\leq 1.3 \times 10^{-7}$ for PF-
35 2M3P, PF-3M2B and 2M3P, respectively, these compounds will have a negligible
36 impact on global warming.

37 **Keywords:** perfluorinated ketones, UV absorption spectrum, IR absorption spectrum,
38 photolysis rates, natural irradiation, atmospheric lifetime, global warming potential.

39 TOC art



40

41 **1. Introduction**

42 Along with hydrofluorocarbons (HFCs), perfluorocarbons (PFCs) are non-ozone
43 depleting substances and therefore excluded from the Montreal Protocol.¹ However,
44 they are considered as greenhouse gases due to their strong absorption in the infrared
45 spectral region in the atmospheric window combined to their long atmospheric
46 lifetimes.² Their atmospheric concentrations have been growing rapidly over last
47 decades and potentially continue to grow.³ They have been widely used for the cooling
48 of power electronics over the last decade. Perfluoroketones such as perfluoro-2-methyl-
49 3-pentanone (PF-2M3P, $C_2F_5C(O)CF(CF_3)_2$, Novec 649/1230) and perfluoro-3-
50 methyl-2-butanone (PF-3M2B, $C_2F_5C(O)CF(CF_3)_2$, Novec5110) are among the
51 important replacement chemicals to halons and CFCs⁴⁻⁵. PF-2M3P and PF-3M2B are
52 advanced heat transfer perfluorocarbons with high dielectric strength. Up to 30 t of PF-
53 2M3P could be released into the atmosphere each year from fire-protection systems⁶.
54 PF-3M2B is being used as versatile insulating gas for medium and high voltage
55 applications including gas insulated lines, gas insulated switchgear and circuit
56 breakers.⁷ The large production and usage of both chemicals are likely to induce their
57 direct emission into the atmosphere.

58

59 Similarly to other volatile organic compounds, PF-2M3P and PF-3M2B may be
60 potentially removed from the atmosphere through photolysis, gas phase chemical
61 reactions with the main atmospheric oxidants, hydrolysis and deposition. The

62 atmospheric fate of PF-2M3P has been subject to a limited number of investigations.
63 Photolysis studies were based on the use of artificial and natural irradiations.^{5,8,9} The
64 atmospheric lifetime of PF-2M3P has been found to be controlled by photolysis and
65 reported to be in the range of 4-14 days depending on latitude and period of the year.⁶
66 The gas phase reactions with OH radical and ozone as well as hydrolysis represent
67 minor contribution to the total removal of PF-2M3P from the atmosphere.⁵⁻⁶ To the
68 best of our knowledge, no experimental data on the photolysis of PF-3M2B have been
69 reported. Hence, the present work aims at investigating the photolysis of PF-3M2B
70 under atmospheric conditions and improving the existing data on PF-2M2B in order to
71 evaluate their atmospheric impacts. In addition to the two perfluorinated ketones, a non-
72 fluorinated analogue aliphatic ketone to PF-2M3P, 2-Methyl-3-pentanone (2M3P,
73 $C_2H_5C(O)CH(CH_3)_2$) has been investigated. The UV-Visible and infrared (IR)
74 absorption spectra of PF-2M3P, PF-3M2B and 2M3P were measured. Their photolysis
75 rates were determined using two complementary atmospheric simulation chambers
76 with natural sunlight irradiation. Atmospheric lifetimes and global warming potentials
77 (GWP) for the three studied compounds are reported and discussed in terms of their
78 atmospheric impacts.

79

80 **2. Experimental Section**

81 **2.1. UV absorption spectra**

82 The apparatus used in this work has been described in previous studies ⁸ and is
83 briefly presented here. The UV-Visible absorption spectra of PF-2M3P, PF-3M2B, and
84 2M3P were measured using a spectrophotometer equipped with a 1200 grooves mm⁻¹
85 grating and a charge-coupled device (CCD) camera. The collimated output of a 30 W
86 deuterium lamp passed through a 100 cm long and 2.5 cm diameter Pyrex absorption
87 cell equipped with quartz windows and focused onto the entrance slit of the
88 spectrometer. Measurements were made over the wavelength region 220–400 nm by
89 recording typically three overlapping regions of about 15 nm. Typically, each
90 measurement consisted of 8-13 scans of diode array. The wavelength scale was
91 calibrated using the emission lines from a low-pressure Hg pen ray lamps (253.7, 313.2,
92 and 365 nm). Absorption cross sections, $\sigma(\lambda)$ (in cm² molecule⁻¹) were obtained using
93 the Beer's law:

$$94 \quad \sigma(\lambda) = \frac{-\ln[I(\lambda)/I_0(\lambda)]}{CL} \quad \text{Eq. 1}$$

95 where L is the path length of absorption cell (in cm), and C is the concentration of the
96 studied compound (in molecule cm⁻³). $I_0(\lambda)$ and $I(\lambda)$ are the light intensities in the
97 absence and in the presence of the compound in the absorption cell, respectively. The
98 concentration of the species of interest in the absorption cell was obtained from the
99 measured pressure using a 0-10 Torr capacitance manometer. Measurements of the PF-
100 2M3P, PF-3M2B and 2M3P UV absorption spectra were performed at $T = (292 \pm 1)$ K
101 using the concentration ranges $[PF-2M3P] = (0.29 - 2.7) \times 10^{17}$, $[PF-3M2B] = (0.27 -$
102 $3.0) \times 10^{17}$ and $[2M3P] = (0.43 - 2.9) \times 10^{17}$ molecule cm⁻³.

103

104 **2.2. Atmospheric simulation chambers**

105 Photolysis studies of PF-2M3P, PF-3M2B and 2M3P were conducted in the large
106 simulation chamber HELIOS. In addition, the photolysis of PF-2M3P was also
107 investigated in a 3.4 m³ Teflon outdoor chamber. Both HELIOS and the 3.4 m³ Teflon
108 outdoor chambers allowed photolysis experiments to be performed under natural solar
109 exposure.

110

111 **2.2.1. HELIOS**

112 The facility consists of a 90 m³ hemispherical outdoor simulation chamber
113 (47°50'18.39N; 1°56'40.03E) made of FEP Teflon film. This facility has been
114 described previously.⁹ The light transmission ranges from 88 to 95% over the entire
115 solar spectrum. Two fans installed in the chamber ensure a rapid mixing of reactants
116 (within less than 90 seconds). Solar actinic flux (290-660 nm) and photolysis
117 frequencies of H₂O₂, HONO, HCHO, NO₃, NO₂ and O(¹D) were measured by a
118 spectroradiometer (Meteorologie Consult GmbH 6007). Pressure, relative humidity and
119 temperature were continuously monitored by a three-axis Ultrasonic Anemometer
120 (Delta Ohm, HD 2003) installed in the center of the chamber. The temperature
121 distribution was also measured using six thermocouples (PT-100) spatially and equally
122 distributed inside the chamber. A mobile protective housing kept the chamber under
123 the dark and can be easily moved to fully expose the chamber to sunlight within 30

124 seconds. The experimental duration under irradiation was between 3 and 7 hours, in
125 which the temperature typically increased by ~ 10 °C. Between experiments, the
126 chamber was cleaned by flushing pure air through for at least 12 hours.

127 Organic compounds were monitored via in situ Fourier transform infrared
128 spectrometry (FT-IR, Bruker Vertex70 spectrometer) coupled to a White-type
129 multipass cell (302.6 m optical path length). Infrared spectra were recorded every 3
130 minutes by co-adding 250 interferograms with a resolution of 0.4 cm^{-1} . The gas phase
131 mixture was also analyzed using a gas chromatography coupled to a mass spectrometer
132 (GC-MS, PekinElmer Clarus 600 C). Gas samples were collected from the chamber at
133 low temperature (-30°C) onto Air Toxics tubes and analyzed through a thermal desorber
134 (TurboMatrix™ 150 ATD), with split mode, followed by a thermal desorption at $300\text{ }^{\circ}\text{C}$
135 (5 min) delivering the sample to a 60-m column (GasPro diameter 0.320mm). The O_3
136 and NO-NO_x concentrations were continuously monitored by UV absorption (HORIBA,
137 APOA 370) and chemiluminescence analyzer (HORIBA, APNA 360), respectively.
138 PF-3M2B was also monitored by PTR-TOF-MS (Proton Transfer Reaction - Time of
139 Flight-Mass Spectrometer, IONICON 8000). The fragment CF_3^+ (m/z 68.986) and
140 $(\text{CF}_3)_2\text{CF}_3^+$ (m/z 168.970) were used to monitor the temporal behavior of PF-3M2B
141 during the photolysis.

142 PF-2M3P and 2M3P were introduced into the chamber by placing known volumes
143 of liquid in a bubbler and then, flushed by purified air. Their concentrations were
144 derived based on the volume of the liquid introduced, the pressure and the temperature

145 in the chamber using the ideal gas law. PF-3M2B and SF₆ were introduced into the
146 chamber by streaming purified air through a calibrated stainless steel cylinder (4.87 L)
147 equipped with capacitance manometers. To compensate sampling flows from analytical
148 instruments and chamber leaks, a flow of purified air (15-25 L/min) was added
149 continuously during all experiments enabling a slight overpressure to be maintained,
150 thus avoiding any contamination from outside air. Dilution of the gas volume in the
151 chamber was determined by monitoring the decay of introduced amount of SF₆
152 (monitored by FT-IR). This decay under dark conditions was found to be in the range
153 of $(5 - 20) \times 10^{-6} \text{ s}^{-1}$.

154 Background concentrations in the chamber were systematically found to be below
155 the detection limits of analytical instruments (e.g., [NO_x] < 2.5 × 10¹⁰, [O₃] < 2.5 × 10¹⁰,
156 [VOC] < 1.3 × 10⁸ molecule cm⁻³).

157

158 **2.2.2. 3.4 m³ outdoor chamber**

159 Photolysis studies of PF-2M3P were also performed in the 3.4 m³ ICARE outdoor
160 atmospheric simulation chamber made of ethylene tetrafluoroethylene (ETFE) foil. The
161 light intensity was continuously monitored using a filter radiometer measuring the
162 photolysis frequency of NO₂, J_{NO_2} (Meteorologie consult GmbH, Germany). The
163 temperature and the relative humidity were also continuously measured using a
164 combined probe (Vaisala HMT330 series transmitters). Chemical analysis of the gas
165 mixture was characterized by an infrared spectrometer (Nicolet 550 Magna FT-IR

166 spectrometer) coupled to a White-type multi-pass mirror cell (optical path length 10
167 meters). Infrared spectra were recorded every 5 minutes by co-adding 130
168 interferograms at a resolution of 1 cm^{-1} . Rapid mixing of reactant was insured using a
169 fan made of Teflon mounted into the chamber. The dilution rate was estimated by
170 monitoring the loss of SF_6 . IR reference spectrum of PF-2M3P was obtained by
171 introducing a known volume of liquid in the chamber. During dark experiments, the
172 chamber was covered by a black and opaque curtain to protect it from sunlight radiation.
173 The curtain could be removed very quickly for exposure to solar radiation, thus
174 initiating the photolysis process. Experiments were performed at 1013 mbar of purified
175 air and in the temperature range of 306 to 319 K. Initial concentrations of PF-2M3P
176 were in the range of $(0.89\text{-}2.7) \times 10^{14}$ molecule cm^{-3} . The gas mixture was exposed to
177 solar irradiation for up to 4 hours.

178

179 **2.3. Photolysis experiments**

180 Under sunlight conditions, the investigated ketones, PF-2M3P, PF-3M2B and
181 2M3P may be removed by photolysis, dilution and wall loss processes following the
182 reactions:



186

187 where J (in s^{-1}) is their photolysis rate while k_L (in s^{-1}) is their decay rates under the
188 dark including dilution and wall loss. Under irradiation, the total decays of the
189 investigated ketones are expressed as follows:

$$190 \quad \ln([\text{ketone}]_0/[\text{ketone}]_t) = k_{\text{tot}} \times t \quad \text{Eq. 2}$$

191 with $[\text{ketone}]_0$ and $[\text{ketone}]_t$ are the concentrations of PF-2M3P or PF-3M2B or 2M3P
192 at times t_0 and t , respectively. k_{tot} (in s^{-1}), the total decay rate of the studied compound
193 under irradiation, is formulated as:

$$194 \quad k_{\text{tot}} = J_{\text{meas}} + k_{\text{d,light}} + (k_L - k_{\text{d,dark}}) \quad \text{Eq. 3}$$

195 J_{meas} is the photolysis rate obtained from the experiment measurement. $k_{\text{d,dark}}$ and
196 $k_{\text{d,light}}$ (in s^{-1}) are, respectively, the dilution decay rates obtained from SF_6 decay in the
197 dark and during irradiation.

198 The atmospheric photolysis rate coefficient was calculated, J_{calc} , as follows:

$$199 \quad J_{\text{calc}} = \int \sigma(\lambda) \Phi(\lambda) F(\lambda) d\lambda \quad (\lambda = 290\text{-}400 \text{ nm}) \quad \text{Eq. 4}$$

200 where $\sigma(\lambda)$, $\Phi(\lambda)$ and $F(\lambda)$ are the absorption cross-section, the quantum yield of
201 dissociation and the actinic flux over the absorption 290 to 400 nm, respectively. The
202 actinic flux was directly measured by the spectroradiometer placed inside the chamber.
203 Assuming a quantum yield of unity for the photodissociation process along the
204 absorption region of PF-2M3P or PF-3M2B or 2M3P, the maximum photolytic rate
205 coefficient can be calculated, $J_{\text{max}} = J_{\text{cal}}$ using Eq. 4. As a result, an effective
206 photodissociation quantum yield can derived:

207
$$\Phi_{\text{eff}} = J_{\text{meas}}/J_{\text{max}} \quad \text{Eq. 5}$$

208

209 **2.4. Chamber loss correction**

210 The concentrations of the products formed from the photolysis of PF-2M3P, PF-
211 3M2B and 2M3P were corrected to account for dilution and possible photolysis/OH
212 reactions under irradiation using the following equation:¹⁰

213
$$[\text{Product}]_{\text{corrected}} = [\text{Product}]_{\text{measured}} \times F \quad \text{Eq. 6}$$

214 with F being the correction factor: $F = 1 + \Delta[\text{Product}]/[\text{Product}]_{\text{measured}}$

215 The amount of product lost, $\Delta[\text{Product}]$ due to secondary reactions, i.e., dilution,
216 reaction with OH radical and photolysis processes is calculated from:

217
$$\Delta[\text{Product}] = \int (k_{\text{d,light}} + J_{\text{product}} + [\text{OH}] \cdot k) \times [\text{Product}]_{\text{measured}} \times dt \quad \text{Eq. 7}$$

218 The losses of CF_3COF , COF_2 and CO were only due to dilution and were corrected
219 using $F < 1.2$. For HCHO , CH_3CHO and CH_3COCH_3 , photolysis, reaction with OH
220 radical and dilution were considered and $F_{\text{HCHO}} < 1.52$, $F_{\text{CH}_3\text{CHO}} < 1.35$ and $F_{\text{CH}_3\text{COCH}_3}$
221 < 1.30 were used for the corresponding corrections. J_{HCHO} measured by the
222 spectroradiometer and $J_{\text{CH}_3\text{CHO}}$ and $J_{\text{CH}_3\text{COCH}_3}$ were calculated using Eq. 4;
223 corresponding $\sigma(\lambda)$ and $\Phi(\lambda)$ values for CH_3CHO and CH_3COCH_3 were taken from
224 IUPAC database¹¹. The OH rate coefficients of CO , HCHO , CH_3CHO and CH_3COCH_3
225 were extracted from IUPAC kinetic database¹¹ as 1.65×10^{-13} , 8.5×10^{-12} , 1.5×10^{-11} and
226 $1.8 \times 10^{-13} \text{ cm}^3 \text{ molecule}^{-1} \text{ s}^{-1}$ at $T = 298 \text{ K}$.

227

228 **2.5 Infrared absorption spectra**

229 The spectra of PF-2M3P, PF-3M2B, and 2M3P were measured at 295 ± 1 K using
230 Fourier transform infrared (FTIR) spectroscopy. Absorption spectra were recorded in
231 250 co-adds between 700 and 4000 cm^{-1} at 1 cm^{-1} resolution (Happ-Genzel apodization).
232 A Whyte-type multi-pass absorption cell with 10 meters optical path length (KBr
233 windows) was used in the course of these measurements. Absorption spectra, $A(\nu)$
234 (base e), (or integrated band strengths) were determined using Beer's law:

$$235 \quad A(\nu) = \sigma(\nu) \times L \times [\text{Ketones}] \quad \text{Eq. 8}$$

236 where $\sigma(\nu)$ is the infrared absorption cross section of the ketones at wavenumber ν , L
237 is the absorption path length, and [ketones] is the PF-2M3P, PF-3M2B, and 2M3P
238 concentration. Measurements were performed using the following concentration ranges
239 (in units of molecule cm^{-3}): $(1.2-10.8) \times 10^{14}$ for PF-2M3P, $(1.6-9.9) \times 10^{14}$ for PF-3M2B
240 and $(0.6-4.8) \times 10^{14}$ for 2M3P. Over the course of the study, replicate measurements
241 were performed using independently prepared gas mixtures with helium as bath gas.
242 The absorption spectra (band strengths) were obtained from a linear least-squares fit of
243 A versus [Ketones] that included at least 6 individual spectrum measurements.

244

245 **2.6. Chemicals**

246 The chemicals used in this work and their stated purities were as follows:
247 perfluoro-2-methyl-3-pentanone (99%, 3M Belgium N.V, Chemical Group-EBC), 2-

248 methyl-3-pentanone (97%, Sigma-Aldrich), perfluoro-3-methyl-2-butanone (98%,
249 Ugarit Chimie), SF₆ (99.9995%, Air Liquide) and O₂ (99.9995%, Air Liquide), Helium
250 (99.9995%, Air Liquide). PF-2M3P, PF-3M2B and 2M3P samples were further
251 purified by using several freeze-pump-thaw cycles. GC-MS analysis of the samples did
252 not show any observable impurities.

253

254 **3. Results and Discussion**

255 **3.1. UV absorption cross section**

256 To test the accuracy of the measurement methodology used in this work, the UV
257 absorption spectrum of acetone has been measured and compared to the recommended
258 UV spectrum from NASA/JPL evaluation.¹² As shown in SI (Figure S1), the level of
259 agreement between both measured and recommended spectra is high, within the
260 measurement accuracy of the recommended UV-Vis absorption spectra ($\approx 8\%$). This
261 excellent agreement provides confidence in the reliability of the absorption cross
262 section measurement conducted in this work.

263 The measured UV-Visible absorption spectra of PF-2M3P, PF-3M2B and 2M3P
264 between 220 and 400 nm at (300 ± 2) K are depicted in Figure 1 and absorption cross
265 sections are provided in Table S1. The quoted uncertainties originated from 2 standard
266 deviation (2σ) of the average of individual measurements. The measurements satisfied
267 Beer's law over a wide concentration range (an order of magnitude). The measured
268 absorbance, A (base e) ranged from 0.2 to 1.7 for PF-2M3P, 0.1 to 1.0 for PF-3M2B,

269 0.3 to 2.0 for 2M3P. Corresponding graphical representations of Beer's law fits are
270 given in Figure S2.

271 2M3P shows a maximum absorption at 284 nm ($\sigma_{(284 \text{ nm})} = (6.99 \pm 0.28) \times 10^{-20}$
272 $\text{cm}^2 \text{ molecule}^{-1}$) while PF-2M3P shows a maximum around 305 nm ($\sigma_{(305 \text{ nm})} = (6.50 \pm$
273 $0.28) \times 10^{-20} \text{ cm}^2 \text{ molecule}^{-1}$) and PF-3M2B exhibits a maximum absorption at 300 nm
274 ($\sigma_{(300 \text{ nm})} = (3.46 \pm 0.15) \times 10^{-20} \text{ cm}^2 \text{ molecule}^{-1}$). The UV absorption spectra obtained
275 in this work are compared with those reported in literature when possible and are
276 presented in Figure 1. The absorption spectrum of PF-2M3P is in agreement with the
277 reported one by Taniguchi et al.,⁵ within 5%. The absorption cross sections of 2M3P
278 obtained in the present work is higher than that reported by Díaz-de-Mera, et al.¹³ by
279 18% (σ_{max}). To the best of our knowledge, the experimental UV spectrum of PF-3M2B
280 is reported for the first time here. Prior to this study, the UV spectrum of PF-3M2B was
281 also determined using a theoretical approach and found to be higher compared to this
282 work, within 27% at the maximum cross section.¹⁴

283 The absorption band of ketones is caused by the dipole forbidden $n\text{-}\pi^*$ transition
284 of the C=O group. The maximum absorption of PF-2M3P is red-shifted, i.e. around 20
285 nm, compared to 2M3P caused by the electronegative substituents in $\alpha\text{-}\alpha'$ -positions.¹⁵⁻
286 ¹⁷ In addition, the maximum absorption of PF-2M3P is about ~2 times higher than that
287 of PF-3M2B, which is consistent with the results of Mu and Mellouki⁸ who observed
288 that the peak UV cross section increased for larger aliphatic ketones.

289 The actinic flux in HELIOS at 13:00 (± 5 min, local time) on 7th of September

290 2013 is also displayed on Figure 1. The integrated absorption cross sections over the
291 actinic flux region for PF-2M3P, 2M3P and PF-3M2B were determined to be 2.61×10^{-18} ,
292 1.22×10^{-18} and 1.25×10^{-18} $\text{cm}^2 \text{ molecule}^{-1}$, respectively, indicating that one could
293 expect $J_{\text{PF-2M3P}} > J_{2\text{M3P}} \approx J_{\text{PF-3M2B}}$.

294

295 3.2. Photolysis of perfluoro-2-methyl-3-pentanone

296 **Photolysis rate measurements.** Experiments in the 3.4 m^3 outdoor chamber were
297 conducted in June-July 2010 at (306-319) K and $\text{RH} < 1\%$. Temporal profiles of PF-
298 2M3P and SF_6 concentrations were monitored under the dark for about 4 hours. No
299 discernible loss other than dilution has been observed; the first order decay rates of PF-
300 2M3P and SF_6 were in the order of $(6.6 - 8.1) \times 10^{-6} \text{ s}^{-1}$. The chamber was then exposed
301 to solar radiation, thus starting the photolysis. The photolysis rate of PF-2M3P, $J_{\text{PF-2M3P}}$,
302 was obtained by considering the total loss of PF-2M3P (k_{tot}) and that from dilution
303 which was obtained from the loss rate of SF_6 (k_d) under irradiation. Experimental details
304 and results derived from the four runs conducted are displayed in Table 1. For all
305 experiments, the photolysis rates of NO_2 were in the range of $(4.4-5.5) \times 10^{-3} \text{ s}^{-1}$. The
306 consumed fractions of PF-2M3P from photodissociation were between 2.1 and 3.7 %
307 and the derived photolysis rates were $(1.7-2.8) \times 10^{-6} \text{ s}^{-1}$ under our experimental
308 conditions ($J_{\text{NO}_2} = (4.4-5.5) \times 10^{-3} \text{ s}^{-1}$). The quoted error corresponds to 2σ obtained from
309 the least square analysis applied on the experimental data. The estimated error on $J_{\text{PF-}}$
310 $_{2\text{M3P}}$ was in the range of 7-14 %.

311 HELIOS experiments were performed during September 2013 at $T = 298 - 317$ K
312 and $RH < 1\%$. SF_6 and PF-2M3P concentrations were monitored by FT-IR and ATD-
313 GC-MS for typically 2 hours in the dark and under natural irradiation for typically 4 to
314 7 hours. The loss rates of SF_6 and PF-2M3P were found to be similar in the dark,
315 equivalent to $(4.8-6.0) \times 10^{-6} \text{ s}^{-1}$, indicating a minor loss on the chamber wall of PF-
316 2M3P. During irradiation, both FT-IR and ATD-GC-MS instruments showed a slightly
317 higher disappearance rate of PF-2M3P than SF_6 which indicated a possible photolysis
318 loss of PF-2M3P (ranging from 1.7 to 7.7 %) under our experimental conditions. The
319 photolysis rate of PF-2M3P, $J_{PF-2M3P}$ was determined to be $(1.1-3.8) \times 10^{-6}$ and $(1.1-$
320 $3.6) \times 10^{-6} \text{ s}^{-1}$ using Eq. 3, from FTIR and GC-MS measurements, respectively, with a
321 recommended range of $(1.1-3.8) \times 10^{-6} \text{ s}^{-1}$ (with $J_{NO_2} = (3.0-5.6) \times 10^{-3} \text{ s}^{-1}$).

322 Table 2 summarizes the photolysis rates of PF-2M3P obtained in this work and
323 those reported in the literature. The values from this work were lower than those
324 reported by D'Anna, et al.¹⁸ Díaz-de-Mera, et al.¹³ who also conducted experiments
325 under natural irradiation in Spain. In contrast, the experiments conducted under
326 artificial irradiation using black lamps or sunlamps led to lower photolysis rate values
327 ⁵. It should be noted that the measured photolysis rate from this work agreed with the
328 result from the TUV model¹⁹ run at different seasons of the year (Table S2).

329 The maximum photolysis rate of PF-2M3P, $J_{\max-PF-2M3P}$, was estimated using
330 absorption cross sections and the actinic flux measured in this work (Eq. 4) and found
331 to be in the range of $(0.7-1.2) \times 10^{-4} \text{ s}^{-1}$. Therefore, the observed photolysis rate

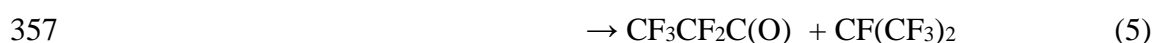
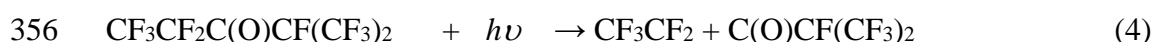
332 corresponds to an effective quantum yield of $\phi_{\text{eff}}=0.015\text{-}0.035$, which is in agreement
333 with the values reported by D'Anna, et al.¹⁸ and Díaz-de-Mera, et al.¹³, 0.043 ± 0.011
334 and 0.044 ± 0.006 , respectively.

335

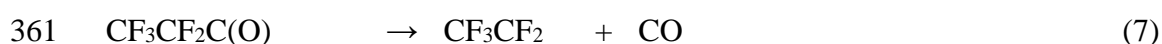
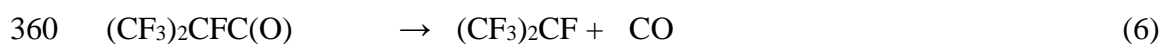
336 **Products and mechanism.** Typical IR spectra obtained from the photolysis of PF-
337 2M3P/SF₆/air mixture in HELIOS are displayed in SI (Figure S3). CF₃COF, COF₂ and
338 CO were identified as photolysis products by FTIR analysis from 3.4 m³ chamber and
339 HELIOS experiments. Perfluoro-propionic acid (CF₃CF₂C(O)OH, PFPrA) and
340 trifluoro-acetic acid (CF₃COOH, TFA) were also identified (m/z 69) among the
341 photolysis products, using the NIST GC-MS library (Figure S4). Temporal profiles of
342 PF-2M3P and its photolysis products are depicted in Figure 2.

343 The formation yields of products (COF₂, CF₃COF and CO) were obtained from a
344 linear least-square fit applied to the experimental data as shown in Figure S5 (HELIOS)
345 and Figure S6 (3.4 m³ chamber) and summarized in Table S3. The recommended
346 formation yields of products ($\pm 2\sigma$) from the photolysis of PF-2M3P are: $(74\pm 18)\%$,
347 $(193\pm 84)\%$, and $(204\pm 68)\%$ for CF₃C(O)F, COF₂, and CO, respectively. The carbon
348 and fluorine budgets were estimated to $(90\pm 28)\%$ and $(57\pm 18)\%$, respectively. This
349 suggests a large fraction of unidentified fluorine-containing products. Indeed,
350 Taniguchi, et al.⁵ identified CF₃O₃CF₃ and CF₃OH as photolysis products that were not
351 identified in the present work.

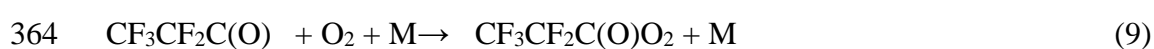
352 A proposed mechanism leading to the formation of the observed products from the
 353 photolysis of PF-2M3P is shown in Figure S7. The photodissociation of PF-2M3P may
 354 occur through a C-C bond cleavage in the α -position of the carbonyl group to produce
 355 perfluoroalkyl and perfluoroacetyl radicals:



358 Perfluoroacetyl radicals are expected to either decompose to give CO and
 359 perfluoroalkyl radical:



362 or react with O₂ leading to the corresponding peroxy radicals:



365 The high formation yield of CO (204±68)% indicates that the thermal
 366 decomposition is an important pathway in the fate of perfluoroacetyl radical over the
 367 reaction with O₂.

368 CF₃COF and COF₂, identified among the photolysis products (74±18)% and
 369 (193±84)%, respectively, might originate from the reactions of CF₃CF₂O₂ and
 370 (CF₃)₂CFCO₂ radicals with RO₂ radicals present in the system leading to the
 371 corresponding RO radicals as (CF₃)₂CFCO and CF₃CF₂O radicals, which would

372 thermally decompose to form CF_3 radicals and the corresponding fluorinated carbonyls
373 $\text{CF}_3\text{C}(\text{O})\text{F}$ and COF_2 .²⁰ In addition, $\text{CF}_3\text{CF}_2\text{OH}$ and CF_3OH , formed from $\text{CF}_3\text{CF}_2\text{O}$
374 and CF_3O radicals reaction with hydrogen-containing compounds present in the
375 chamber (e.g., HCHO desorbing from the chamber walls, impurities in the air diluent,
376 or water), were also reported to transform rapidly into COF_2 .²¹⁻²²

377

378 3.3. Photolysis of 2-methyl-3-pentanone

379 **Photolysis rate measurements.** Mixtures of 2M3P/ SF_6 /air were added into
380 HELIOS and left in the dark typically for 2 hours before irradiation by solar light. The
381 loss rates of SF_6 and 2M3P in the dark were determined to be $(4.8-6.2) \times 10^{-6}$ and $(5.2-$
382 $6.8) \times 10^{-6} \text{ s}^{-1}$, respectively. The chemical mixture 2M3P/ SF_6 /air was then exposed to
383 solar irradiation for typically 5-6 hours. Under these experimental conditions, the
384 measured loss of 2M3P ranged from 3.9 to 6.3%. The determination of $J_{2\text{M3P}}$ from FTIR
385 and GC-MS measurements were in good agreement, within (3-7) %. The experimental
386 conditions and the obtained values of $J_{2\text{M3P}}$ are summarized in Table 1.

387 All the experiments were performed in the absence of OH radical scavenger to
388 avoid spectral interferences in the mid-infrared region with the studied compounds.
389 Therefore, the gas phase removal of 2M3P during solar exposure might also due to the
390 reaction of OH radicals with 2M3P in addition to its photolysis. Indeed, when the
391 chamber was only filled with purified air and exposed to solar irradiation, separate
392 measurements using a chemical ionization mass spectrometer (CIMS) have shown the

393 presence of OH radicals at concentration ranging from $(2.1\pm 0.9)\times 10^5$ occasionally up
394 to 2×10^6 molecule cm^{-3} could be observed. This implied that under these conditions,
395 the OH reaction contribution to the total loss of 2M3P would have contributed from 30%
396 to 100%. However, it has been also observed that the disappearance rate of 2M3P
397 during solar exposure during this study was very comparable to those of PF-2M3P and
398 PF-3M2B (Table 1), suggesting that the OH concentration level during these
399 experiments was very low. Therefore, in the absence of OH radical direct measurement
400 during this study, we preferred to be conservative and thus, recommend an upper limit
401 for the photolysis rate of 2M3P, equivalent to $(2.6\pm 1.4)\times 10^{-6}$ s^{-1} (with $J_{\text{NO}_2} = 5.6\times 10^{-3}$
402 s^{-1}).

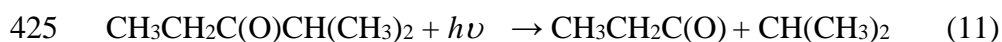
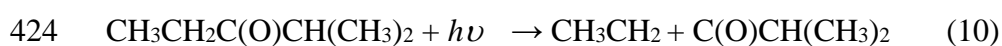
403 Based on the integrated UV absorption spectrum over the actinic flux region, the
404 derived maximum photolysis rate constant of 2M3P, $J_{\text{max-2M3P}}$, was found to be $(6.5-$
405 $9.6)\times 10^{-6}$ s^{-1} . Therefore, the effective photolysis quantum yield is estimated to be ϕ_{eff}
406 ≤ 0.28 under tropospheric sunlight conditions.

407

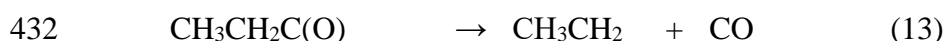
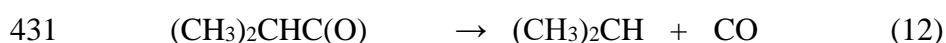
408 **Products and mechanism.** Products were identified and quantified using FT-IR
409 spectroscopy. The Figure S8 displays the typical spectra acquired before and after the
410 photolysis of 2M3P. Comparison of measured calibrated IR spectra shows the presence
411 of CH_3CHO , CO , CH_3COCH_3 and HCHO among the oxidation products where an
412 example of time-concentration profiles of 2M3P and its products is shown in Figure S9.
413 These products have been observed to be of primary origin when 2M3P was exposed

414 to natural irradiation (Figure S10). As explained previously, derived formation yields
 415 of products, possibly accounted for both contributions of photolysis and OH reactions,
 416 were estimated to (81±18)%, (25±6)%, (90±16)% and (98±10)% for CH₃CHO, HCHO,
 417 CH₃COCH₃ and CO, respectively.-Therefore, due to unquantified contribution of OH
 418 reaction to the formation yields of products during this photolysis study, we prefer to
 419 conclude qualitatively on the formation of CH₃CHO, HCHO, CH₃COCH₃ and CO
 420 among the photolysis products from the irradiation of 2M3P.

421 Figure S11 shows the proposed mechanistic pathways leading to the formation of
 422 the observed products. The photolysis of 2M3P may occur via C-C bond cleavage
 423 associated with C=O group to form an alkyl and the corresponding acetyl radical:



426 CH₃CH₂C(O) and C(O)CH(CH₃)₂ radicals, are expected to either decompose to
 427 alkyl radicals (CH₃CH₂ and (CH₃)₂CH) leading to CO elimination or react with O₂ to
 428 form the corresponding acetyl peroxy radicals ((CH₃)₂CHC(O)O₂ and CH₃CH₂C(O)O₂).
 429 CO formation indicating the occurrence of at least one of the decomposition channels
 430 12 and 13:



433 The reaction of CH₃CH₂C(O)O₂ with HO₂ radical has been reported to lead to
 434 the formation of CH₃CH₂C(O)OH and O₃.²³ However, the absence of the carboxylic

435 acid and O₃ among the photolysis products indicates that the reaction of acetyl peroxy
436 radicals with HO₂ was insignificant under our experimental conditions. CH₃CH₂C(O)O
437 and (CH₃)₂CHC(O)O radicals are expected to decompose to form the corresponding
438 alkyl radicals, CH₃CH₂ and (CH₃)₂CH, respectively.²³⁻²⁴

439 As shown in Figure S11, the subsequent reaction of CH₃CH₂ and (CH₃)₂CH with
440 O₂ would form the corresponding peroxy radicals, CH₃CH₂O₂ and (CH₃)₂CHO₂. The
441 self-reaction of CH₃CH₂O₂ radical would lead to the formation of CH₃CH₂O radical
442 (60%) and CH₃CHO + CH₃CH₂OH (40%).¹² In addition, the (CH₃)₂CHO₂ radical self-
443 reaction would lead to the formation of (CH₃)₂CHO radical (60%) and CH₃C(O)CH₃ +
444 (CH₃)₂CHOH (40%). CH₃CH₂O and (CH₃)₂CHO alkoxy radicals are expected to react
445 with O₂ to form HCHO, CH₃CHO and CH₃C(O)CH₃.

446

447 **3.4. Photolysis of perfluoro-3-methyl-2-butanone**

448 PF-3M2B/SF₆/air mixtures were monitored for 2 hours in the dark in HELIOS.
449 The dark loss rates of SF₆ and PF-3M2B were similar and found to be (1.1-1.3) × 10⁻⁵
450 s⁻¹. The gas mixture PF-3M2B /SF₆/air was exposed to solar irradiation for typically 5-
451 6 hours. PF-3M2B was monitored by FTIR and PTR-TOF-MS (CF₃⁺ and (CF₃)₂CF₃⁺
452 ions at *m/z* 68.986 and *m/z* 168.970, respectively). The observed loss of PF-3M2B
453 ranged from 1.3 to 2.0% depending on the solar light intensity. The obtained photolysis
454 rate was $J_{\text{PF-3M2B}} = (9 \pm 5) \times 10^{-7} \text{ s}^{-1}$ with $J_{\text{NO}_2} = (4.2-7.7) \times 10^{-3} \text{ s}^{-1}$. The experimental
455 conditions and the corresponding results are summarized in Table 1. The TUV model

456 was also used to calculate the PF-3M2B photolysis loss rates at the different period of
457 year, ranging from $2 \times 10^{-7} \text{ s}^{-1}$ to $1.2 \times 10^{-6} \text{ s}^{-1}$. No detectable formation of products was
458 observed from the photolysis of PF-3M2B due to its low photolysis rate and to the
459 detection limits of the analytical techniques used.

460 The maximum photolysis rate constant of PF-3M2B, $J_{\text{max-PF-3M2B}}$, was estimated
461 using the integrated UV absorption spectrum over the actinic flux region and found to
462 be $J_{\text{max-PF-3M2B}} = (2.9-5.6) \times 10^{-5} \text{ s}^{-1}$. The measured photolysis rate led to an effective
463 photolysis quantum yield estimated to $\phi_{\text{eff}} \leq 0.037$ under tropospheric sunlight
464 conditions.

465

466 **3.5 Infrared absorption and global warming potential (GWP)**

467 The infrared absorption spectra of the PF-2M3P and PF-3M2B measured in this
468 work are characterized by broad diffuse vibrational bands as shown in Figure 3,
469 (digitized absorption spectra are provided in SI as .txt format). The spectra are
470 characterized by strong absorption features in the C-F stretch regions, $1200-1400 \text{ cm}^{-1}$.
471 Overall, the larger perfluorinated ketones have greater peak cross sections in this region
472 due, in part, to the greater overlap of vibrational bands. The infrared spectrum of 2M3P
473 is also characterized by broad vibrational band, due to absorption features of C-H
474 stretch regions. The IR spectrum of 2M3P is also characterized by a sharp absorption
475 at 1700 cm^{-1} , corresponding to C=O stretch vibration (Figure 3). Corresponding
476 graphical representations of Beer's law fits are given in Figures S12, S13 and S14.

477 The integrated band strengths over the 700-2000 cm^{-1} region were determined
478 to be 3.68×10^{-16} , 3.03×10^{-16} and 1.0×10^{-16} $\text{cm}^2 \text{ molecule}^{-1} \text{ cm}^{-1}$ (base *e*) for PF-2M3P,
479 PF-3M2B and 2M3P, respectively. Integrated band strengths of PF-2M3P over the 700-
480 2000 cm^{-1} IR spectral region reported by Díaz-de-Mera, et al. ¹³ (3.94×10^{-16} cm^2
481 $\text{molecule}^{-1} \text{ cm}^{-1}$) and D'Anna, et al. ¹⁸ (4.05×10^{-16} $\text{cm}^2 \text{ molecule}^{-1} \text{ cm}^{-1}$) are in
482 agreement with the present results, within 7% and 9%, respectively. To the best of our
483 knowledge, IR spectra of PF-3M2B and 2M3P are reported for the first time in this
484 work.

485 The radiative efficiencies (RE) for the investigated ketones were calculated
486 using the experimentally measured spectra and the method given in Hodnebrog, et al.
487 ²⁵. The RE values obtained in this work are 0.357, 0.304 and 1.78×10^{-6} $\text{W m}^{-2} \text{ ppbv}^{-1}$
488 for PF-2M3P, PF-3M2B and 2M3P, respectively for atmospherically well-mixed
489 conditions and + 10% stratospheric temperature correction.

490 However, the radiative forcing for the present ketones is expected to be minor
491 due to their expected short atmospheric lifetimes, < 13 days, and low atmospheric
492 abundances. Therefore, lifetime-adjusted RE, accounting for non-uniform horizontal
493 and vertical mixing for very short-lived compounds, was preferred and calculated to be
494 0.012-0.036, ~ 0.036 and $\leq 4 \times 10^{-8}$ $\text{W m}^{-2} \text{ ppbv}^{-1}$ for PF-2M3P, PF-3M2B and 2M3P,
495 respectively. Corresponding GWPs (for 100 years horizon) were found to be <0.21,
496 ~ 0.29 and $\leq 1.3 \times 10^{-7}$ for PF-2M3P, PF-3M2B and 2M3P, respectively, showing a
497 minor contribution of the studied ketones to the global warming potential. As shown in

498 Table S4, GWP of PF-2M3P is in good agreement with the studies of Díaz-de-Mera, et
499 al.¹³ and Hodnebrog, et al.²⁵.

500

501 **4. Atmospheric implications**

502 The photolysis rate of PF-2M3P was measured in September 2013 and July
503 2010 under natural irradiation and found to be $(1.1-3.8) \times 10^{-6} \text{ s}^{-1}$ and $(1.7-2.8) \times 10^{-6} \text{ s}^{-1}$,
504 respectively ($J_{\text{NO}_2} = (3.3-5.6) \times 10^{-3} \text{ s}^{-1}$) leading to an atmospheric lifetime of PF-2M3P
505 with respect to photolysis in the range of 3-11 days considering that the photolysis
506 occurs during the daytime, which is in good agreement with the literature results, i.e.,
507 4-14 days.^{5-6, 13, 18} The hydrolysis as removal process was demonstrated to be too slow
508 to be considered of atmospheric importance.⁵⁻⁶ Besides, due to a high air-water partition
509 coefficient,²⁶ very low quantities of PF-2M3P will be present in the cloud droplets.
510 Based on the upper limits for the reaction rate coefficients (in units of $\text{cm}^3 \text{ molecule}^{-1}$
511 s^{-1}) with OH radical ($<5 \times 10^{-16}$), O_3 ($<4 \times 10^{-22}$) and Cl atoms ($<1.7 \times 10^{-19}$) taken from
512 Taniguchi, et al.⁵ and typical global average tropospheric concentrations (in molecule
513 cm^{-3}) of OH $\sim 2 \times 10^6$,²⁷ Cl $\sim 10^4$,²⁸ and $\text{O}_3 \sim 7 \times 10^{11}$,²⁹ the tropospheric lifetime towards
514 OH, Cl and O_3 reactions is equivalent to > 30 years. Thus, it is concluded that the
515 photolysis will be the dominant atmospheric loss process for PF-2M3P.

516 Based on the photolysis rate measurement of PF-3M2B under natural irradiation
517 ($J_{\text{PF-3M2B}} = (9 \pm 5) \times 10^{-7} \text{ s}^{-1}$), an atmospheric lifetime with respect to photolysis of ~ 13
518 days was derived. To the best of our knowledge, this work provides the first photolysis

519 study of PF-3M2B. By analogy with PF-2M3P, other processes such as reactions with
520 OH radical, Cl and O₃ and hydrolysis would not contribute significantly to the
521 atmospheric removal of PF-3M2B.

522 Using the photolysis rates of 2M3P measured under natural irradiation ($J_{2M3P} =$
523 $\leq(2.6\pm 1.4)\times 10^{-6} \text{ s}^{-1}$), an atmospheric lifetime with respect to photolysis of ≥ 4 days was
524 derived. In addition to photolysis, gas phase reactions with OH radical and Cl atom
525 could also contribute significantly to the tropospheric loss of 2M3P. Indeed,
526 tropospheric lifetimes towards OH and Cl reactions were derived to be ≈ 4 (OH rate
527 coefficient estimated from SAR)³⁰ and 11 days³¹, respectively. Thus, both photolysis
528 and gas phase loss processes will contribute to the loss of 2M3P in the troposphere.
529 Therefore, the tropospheric lifetime, τ_{tot} , defined as $\frac{1}{\tau_{tot}} = \frac{1}{\tau_{OH}} + \frac{1}{\tau_{Cl}} + \frac{1}{\tau_{hv}}$ with τ_{OH} , τ_{Cl}
530 and τ_{OH} , the corresponding lifetimes with respect to photolysis and OH radical and Cl
531 reactions, respectively, was estimated to be 1-2 days.

532 Based on the present study, the photolysis of PF-2M3P has been found to produce
533 CF₃C(O)F, COF₂, TFA, PFPrA, and CO under natural conditions. In the atmosphere,
534 CF₃C(O)F will mainly hydrolyze to give trifluoroacetic acid (TFA, CF₃C(O)OH). In
535 the lower atmosphere, COF₂ will be lost through hydrolysis,³²⁻³³ whereas in the
536 stratosphere, the photolysis is the dominant pathway producing CO₂ and HF,³⁴ leading
537 to a local lifetime of 5-10 days.³⁵

538 The photolysis of 2M3P in the troposphere will lead to the formation of
539 CH₃C(O)CH₃, CH₃CHO, HCHO and CO. The major atmospheric loss of CH₃C(O)CH₃,

540 CH₃CHO and HCHO is controlled by photolysis and reaction with OH radical. Their
541 photolysis are a source of HO_x (OH, HO₂) in the upper troposphere.^{16,36}

542 Finally, the low GWP values and the short atmospheric lifetimes for the studied
543 ketones may not lead to a large impact on the global warming of the Earth's atmosphere
544 but may have some impact regarding the formation of other fluorinated species.

545

546 **ASSOCIATED CONTENT**

547 **Supporting Information**

548 UV absorption cross section of PF-2M3P, PF-3M2B and 2M3P are provided in Table
549 S1 and Beer's law fits in Figure S2; UV absorption spectra of acetone is displayed in
550 Figure S1; Seasonal dependence of the photolysis rate of PF-2M3P, PF-3M2B and
551 2M3P simulated using TUV Model is tabulated in Table S2; Figures S3 and S4
552 represents the FTIR spectra and GC-MS spectrum, respectively and were used to obtain
553 the products yield as shown in Figures S5 and S6. Formation yields from the photolysis
554 of PF-2M3P are summarized in Table S3. Corresponding photolysis pathway is
555 proposed in Figure S7; Figure S8 presents the FTIR spectra from irradiation of 2M3P.
556 Figure S10 presents the data used to derive the formation yield of products from the
557 loss of 2M3P (Figure S9). Corresponding proposed photolysis pathway is given in
558 Figure S11. Infrared absorption cross sections of 2M3P, PF-2M3P and PF-3M2B (.txt
559 format) used to calculate radiative efficiencies (RE) and GWPs (100 years) (Table S4)
560 and the fitting according to Beer's law (Figure S12, Figure 13 and Figure S14).

561

562 **AUTHOR INFORMATION**

563 **Corresponding Author**

564 *Tel: 33 (0)2 38 25 76 12; e-mail: mellouki@cnrs-orleans.fr.

565 **ORCID**

566 Yangang Ren: 0000-0001-5770-5050

567 François Bernard: 0000-0002-6116-3167

568 Véronique Daële: 0000-0003-2509-4077

569 Abdelwahid Mellouki: 0000-0002-6594-5262

570

571

572

573 **Acknowledgments**

574 This work is supported by Labex Voltaire (ANR-10-LABX-100-01), ARD PIVOTS
575 program (supported by the Centre-Val de Loire regional council), and the European
576 Union's Horizon 2020 research and innovation programme through the
577 EUROCHAMP-2020 Infrastructure Activity under grant agreement No. 730997.
578

579 **References**

- 580 (1) Forrest, E. C.; Hu, L.-W.; Buongiorno, J.; McKrell, T. J., Pool Boiling Heat
581 Transfer Performance of a Dielectric Fluid With Low Global Warming Potential. *Heat*
582 *Transfer Eng.* **2013**, *34* (15), 1262-1277.
- 583 (2) Yao, B.; Vollmer, M. K.; Zhou, L. X.; Henne, S.; Reimann, S.; Li, P. C.; Wenger,
584 A.; Hill, M., In-situ measurements of atmospheric hydrofluorocarbons (HFCs) and
585 perfluorocarbons (PFCs) at the Shangdianzi regional background station, China. *Atmos.*
586 *Chem. Phys.* **2012**, *12* (21), 10181-10193.
- 587 (3) Schaefer, D. O.; Godwin, D.; Harnisch, J., Estimating Future Emissions and
588 Potential Reductions of HFCs, PFCs, and SF₆. *Energy J.* **2006**, *27*, 63-88.
- 589 (4) Hyrenbach, M. In *Alternative gas insulation in medium-voltage switchgear*, 23rd
590 International Conference on Electricity Distribution, Lyon, 15-18 June; Lyon, 2015.
- 591 (5) Taniguchi, N.; Wallington, T. J.; Hurley, M. D.; Guschin, A. G.; Molina, L. T.;
592 Molina, M. J., Atmospheric Chemistry of C₂F₅C(O)CF(CF₃)₂: Photolysis and Reaction
593 with Cl Atoms, OH Radicals, and Ozone. *J. Phys. Chem. A* **2003**, *107* (15), 2674-2679.
- 594 (6) Jackson, D. A.; Young, C. J.; Hurley, M. D.; Wallington, T. J.; Mabury, S. A.,
595 Atmospheric Degradation of Perfluoro-2-methyl-3-pentanone: Photolysis, Hydrolysis
596 and Hydration. *Environ. Sci. Technol.* **2011**, *45* (19), 8030-8036.
- 597 (7) Hyrenbach, M.; Zache, S. In *Alternative insulation gas for medium-voltage*
598 *switchgear*, 2016 Petroleum and Chemical Industry Conference Europe (PCIC Europe),
599 14-16 June 2016; 2016; pp 1-9.
- 600 (8) Mu, Y. J.; Mellouki, A., The near-UV absorption cross sections for several ketones.
601 *J. Photochem. Photobiol., A* **2000**, *134* (1-2), 31-36.
- 602 (9) Ren, Y.; Grosselin, B.; Daele, V.; Mellouki, A., Investigation of the reaction of
603 ozone with isoprene, methacrolein and methyl vinyl ketone using the HELIOS
604 Chamber. *Faraday Discussions* **2017**, *200* (0), 289-311.
- 605 (10) Volkamer, R.; Platt, U.; Wirtz, K., Primary and Secondary Glyoxal Formation
606 from Aromatics: Experimental Evidence for the Bicycloalkyl-Radical Pathway from
607 Benzene, Toluene, and p-Xylene. *J. Phys. Chem. A* **2001**, *105* (33), 7865-7874.
- 608 (11) Atkinson, R.; Baulch, D. L.; Cox, R. A.; Crowley, J. N.; Hampson, R. F.; Hynes,
609 R. G.; Jenkin, M. E.; Rossi, M. J.; Troe, J.; Subcommittee, I., Evaluated kinetic and
610 photochemical data for atmospheric chemistry: Volume II – gas phase reactions
611 of organic species. *Atmos. Chem. Phys.* **2006**, *6* (11), 3625-4055.
- 612 (12) J. B. Burkholder; S. P. Sander; J. Abbatt; J. R. Barker; R. E. Huie; C. E. Kolb; M.
613 J. Kurylo; V. L. Orkin; D. M. Wilmouth; Wine, P. H., Chemical Kinetics and
614 Photochemical Data for Use in Atmospheric Studies, Evaluation No. 18. JPL
615 Publication 15-10, J. P. L., Ed. Pasadena,, 2015.
- 616 (13) Díaz-de-Mera, Y.; Aranda, A.; Notario, A.; Rodriguez, A.; Rodriguez, D.; Bravo,
617 I., Photolysis study of fluorinated ketones under natural sunlight conditions. *Phys.*
618 *Chem. Chem. Phys.* **2015**, *17* (35), 22991-22998.

- 619 (14) Yu, X.; Hou, H.; Wang, B., Atmospheric Chemistry of Perfluoro-3-methyl-2-
620 butanone [CF₃C(O)CF(CF₃)₂]: Photodissociation and Reaction with OH Radicals. *J.*
621 *Phys. Chem. A* **2018**, *122* (45), 8840-8848.
- 622 (15) Chiappero, M. S.; Malanca, F. E.; Argüello, G. A.; Wooldridge, S. T.; Hurley, M.
623 D.; Ball, J. C.; Wallington, T. J.; Waterland, R. L.; Buck, R. C., Atmospheric Chemistry
624 of Perfluoroaldehydes (C_xF_{2x+1}CHO) and Fluorotelomer Aldehydes
625 (C_xF_{2x+1}CH₂CHO): Quantification of the Important Role of Photolysis. *J. Phys. Chem.*
626 *A* **2006**, *110* (43), 11944-11953.
- 627 (16) Simpson, W. R.; von Glasow, R.; Riedel, K.; Anderson, P.; Ariya, P.; Bottenheim,
628 J.; Burrows, J.; Carpenter, L. J.; Frieß, U.; Goodsite, M. E.; Heard, D.; Hutterli, M.;
629 Jacobi, H. W.; Kaleschke, L.; Neff, B.; Plane, J.; Platt, U.; Richter, A.; Roscoe, H.;
630 Sander, R.; Shepson, P.; Sodeau, J.; Steffen, A.; Wagner, T.; Wolff, E., Halogens and
631 their role in polar boundary-layer ozone depletion. *Atmos. Chem. Phys.* **2007**, *7* (16),
632 4375-4418.
- 633 (17) Metcalfe, J.; Phillips, D., Photophysical processes in fluorinated acetones. *J.*
634 *Chem. Soc., Faraday Trans. 2*, **1976**, *72* (0), 1574-1583.
- 635 (18) D'Anna, B.; Sellevåg, S. R.; Wirtz, K.; Nielsen, C. J., Photolysis Study of
636 Perfluoro-2-methyl-3-pentanone under Natural Sunlight Conditions. *Environ. Sci.*
637 *Technol.* **2005**, *39* (22), 8708-8711.
- 638 (19) Madronich, S.; Flocke, S., The Role of Solar Radiation in Atmospheric Chemistry.
639 In *Environmental Photochemistry*, Boule, P., Ed. Springer Berlin Heidelberg: Berlin,
640 Heidelberg, 1999; pp 1-26.
- 641 (20) Sehested, J.; Ellermann, T.; Nielsen, O. J.; Wallington, T. J.; Hurley, M. D., UV
642 Absorption Spectrum, and Kinetics and Mechanism of the Self Reaction of CF₃CF₂O₂
643 Radicals in the Gas Phase at 295 K. *Int. J. Chem. Kinet.* **1993**, *25* (9), 701-717.
- 644 (21) Wallington, T. J.; Hurley, M. D.; Schneider, W. F.; Sehested, J.; Nielsen, O. J.,
645 Atmospheric chemistry of trifluoromethoxy radicals: reaction with water. *J. Phys.*
646 *Chem.* **1993**, *97* (29), 7606-7611.
- 647 (22) Young, C. J.; Donaldson, D. J., Overtone-Induced Degradation of Perfluorinated
648 Alcohols in the Atmosphere. *J. Phys. Chem. A* **2007**, *111* (51), 13466-13471.
- 649 (23) Le Crâne, J.-P.; Villenave, E.; Hurley, M. D.; Wallington, T. J.; Ball, J. C.,
650 Atmospheric Chemistry of Propionaldehyde: Kinetics and Mechanisms of Reactions
651 with OH Radicals and Cl Atoms, UV Spectrum, and Self-Reaction Kinetics of
652 CH₃CH₂C(O)O₂ Radicals at 298 K. *J. Phys. Chem. A* **2005**, *109* (51), 11837-11850.
- 653 (24) Lightfoot, P. D.; Cox, R. A.; Crowley, J. N.; Destriau, M.; Hayman, G. D.; Jenkin,
654 M. E.; Moortgat, G. K.; Zabel, F., Organic peroxy-radicals-kinetics, spectroscopy and
655 tropospheric chemistry. *Atmos. Environ.* **1992**, *26* (10), 1805-1961.
- 656 (25) Hodnebrog, Ø.; Etminan, M.; Fuglestad, J. S.; Marston, G.; Myhre, G.; Nielsen,
657 C. J.; Shine, K. P.; Wallington, T. J., Global warming potentials and radiative
658 efficiencies of halocarbons and related compounds: A comprehensive review. *Rev.*
659 *Geophys.* **2013**, *51* (2), 300-378.

660 (26) Rayne, S.; Forest, K., Prediction of the air-water partition coefficient for
661 perfluoro-2-methyl-3-pentanone using high-level Gaussian-4 composite theoretical
662 methods. *J. Environ. Sci. Health., Part A* **2014**, *49* (11), 1228-1235.

663 (27) Hein, R.; Crutzen, P. J.; Heimann, M., An inverse modeling approach to
664 investigate the global atmospheric methane cycle. *Global Biogeochem. Cycles* **1997**,
665 *11* (1), 43-76.

666 (28) Saiz-Lopez, A.; von Glasow, R., Reactive halogen chemistry in the troposphere.
667 *Chem. Soc. Rev.* **2012**, *41* (19), 6448-6472.

668 (29) Monks, P. S.; Granier, C.; Fuzzi, S.; Stohl, A.; Williams, M. L.; Akimoto, H.;
669 Amann, M.; Baklanov, A.; Baltensperger, U.; Bey, I.; Blake, N.; Blake, R. S.; Carslaw,
670 K.; Cooper, O. R.; Dentener, F.; Fowler, D.; Fragkou, E.; Frost, G. J.; Generoso, S.;
671 Ginoux, P.; Grewe, V.; Guenther, A.; Hansson, H. C.; Henne, S.; Hjorth, J.;
672 Hofzumahaus, A.; Huntrieser, H.; Isaksen, I. S. A.; Jenkin, M. E.; Kaiser, J.; Kanakidou,
673 M.; Klimont, Z.; Kulmala, M.; Laj, P.; Lawrence, M. G.; Lee, J. D.; Liousse, C.; Maione,
674 M.; McFiggans, G.; Metzger, A.; Mieville, A.; Moussiopoulos, N.; Orlando, J. J.;
675 O'Dowd, C. D.; Palmer, P. I.; Parrish, D. D.; Petzold, A.; Platt, U.; Pöschl, U.; Prévôt,
676 A. S. H.; Reeves, C. E.; Reimann, S.; Rudich, Y.; Sellegri, K.; Steinbrecher, R.;
677 Simpson, D.; ten Brink, H.; Theloke, J.; van der Werf, G. R.; Vautard, R.; Vestreng, V.;
678 Vlachokostas, C.; von Glasow, R., Atmospheric composition change – global and
679 regional air quality. *Atmos. Environ.* **2009**, *43* (33), 5268-5350.

680 (30) Kwok, E. S. C.; Atkinson, R., Estimation of hydroxyl radical reaction rate
681 constants for gas-phase organic compounds using a structure-reactivity relationship: An
682 update. *Atmos. Environ.* **1995**, *29* (14), 1685-1695.

683 (31) Ren, Y.; Wang, J.; Grosselin, B.; Daële, V.; Mellouki, A., Kinetic and product
684 studies of Cl atoms reactions with a series of branched Ketones. *J. Environ. Sci.* **2018**,
685 *71*, 271-282.

686 (32) Houde, M.; Martin, J. W.; Letcher, R. J.; Solomon, K. R.; Muir, D. C. G.,
687 Biological Monitoring of Polyfluoroalkyl Substances: A Review. *Environ. Sci.*
688 *Technol.* **2006**, *40* (11), 3463-3473.

689 (33) Hanson, D. R.; Ravishankara, A. R., The loss of CF₂O on Ice, Nat, and Sulfuric-
690 acid-solutions. *Geophys. Res. Lett.* **1991**, *18* (9), 1699-1701.

691 (34) Nolle, A.; Krumscheid, C.; Heydtmann, H., Determination of quantum yields in
692 the UV photolysis of COF₂ and COFCl. *Chem. Phys. Lett.* **1999**, *299* (6), 561-565.

693 (35) WMO (World Meteorological Organization) *Scientific Assessment of Ozone*
694 *Depletion: 2010, Global Ozone Research and Monitoring Project–Report*; Switzerland,
695 Geneva, 2011; p 516

696 (36) Jaegle, L.; Jacob, D. J.; Brune, W. H.; Wennberg, P. O., Chemistry of HO_x
697 radicals in the upper troposphere. *Atmos. Environ.* **2001**, *35* (3), 469-489.

698
699

700 **Table 1.** Experimental conditions and obtained results for the photolysis of perfluoro-
 701 2-methyl-3-pentanone (PF-2M3P), perfluoro-3-methyl-2-butanone (PF-3M2B) and 2-
 702 methyl-3-pentanone (2M3P).

[ketone]	J_{NO_2} (10^{13} molecule cm^{-3})	Photolysis loss (%)	Irradiation period (h:mm)	J (10^{-6} s^{-1})			
				FT-IR	GC-MS ^b / PTR-TOF-MS ^c	Rec ^a	
3.4 m ³ outdoor chamber							
	18	4.4±1.1	3.7	4:23	2.3±0.2	-	2.3±0.4
	18	4.9±0.9	3.7	4:18	2.8±0.2	-	2.8±0.4
	27	4.4±1.5	2.1	3:39	1.7±0.2	-	1.7±0.4
	8.9	5.5±0.6	2.8	4:13	1.9±0.3	-	1.9±0.6
PF-2M3P	HELIOS						
	3.8	3.0±0.4	1.7	4:32	1.1±0.1	1.1±0.1 ^b	1.1±0.4
	3.0	5.3±1.0	7.7	5:01	3.8±0.3	3.5±0.5 ^b	3.8±1.0
	3.6	4.6±1.2	6.1	7:11	2.2±0.3	2.3±0.4 ^b	2.2±0.8
	3.5	5.6±0.7	7.4	7:08	3.7±0.5	3.6±0.5 ^b	3.6±1.0
	3.3	2.9±1.2	5.7	6:00	1.6±0.7	1.5±0.4 ^b	1.6±1.0
	3.4	2.2±0.3	3.9	5:49	1.2±0.2	1.3±0.4 ^b	1.2±0.8
2M3P	3.4	2.4±1.1	3.9	6:14	1.5±0.2	1.7±0.3 ^b	1.6±0.6
	3.3	5.6±0.5	6.3	5:26	2.7±0.7	2.6±0.7 ^b	2.6±1.4
	3.4	5.1±0.5	5.3	6:01	2.1±0.7	2.0±0.4 ^b	2.0±1.0
	3.4	5.1±0.7	4.8	4:58	2.0±0.6	2.0±0.4 ^b	2.0±1.2
	0.09	7.6±1.3	< 0.2%	5:30	< 1%	-	
	0.05	7.7±1.4	< 0.2%	5:17	< 1%	-	
PF-3M2B	1.5	4.2±1.8	2.0	5:07	1.1	-	1.1
	4.2	5.8±1.1	1.3	5:30	0.67	0.28 ^c	0.48±0.28
	3.9	6.3±1.4	1.7	6:08	0.8	1.2 ^c	0.98±0.50

703 ^a Recommended value obtained from the weighted average of each individual
 704 measurement: $J_{\text{av}}=(w_1J_1+ w_2J_2 + \dots)/(w_1+ w_2+\dots)$, where $w=1/\sigma^2$, etc. The error, is
 705 given by: $2\sigma_{\text{av}}=(\sigma_1^2+\sigma_2^2+ \dots)^{0.5}$

706 ^b measured using GC-MS

707 ^c measured using PTR-TOF-MS

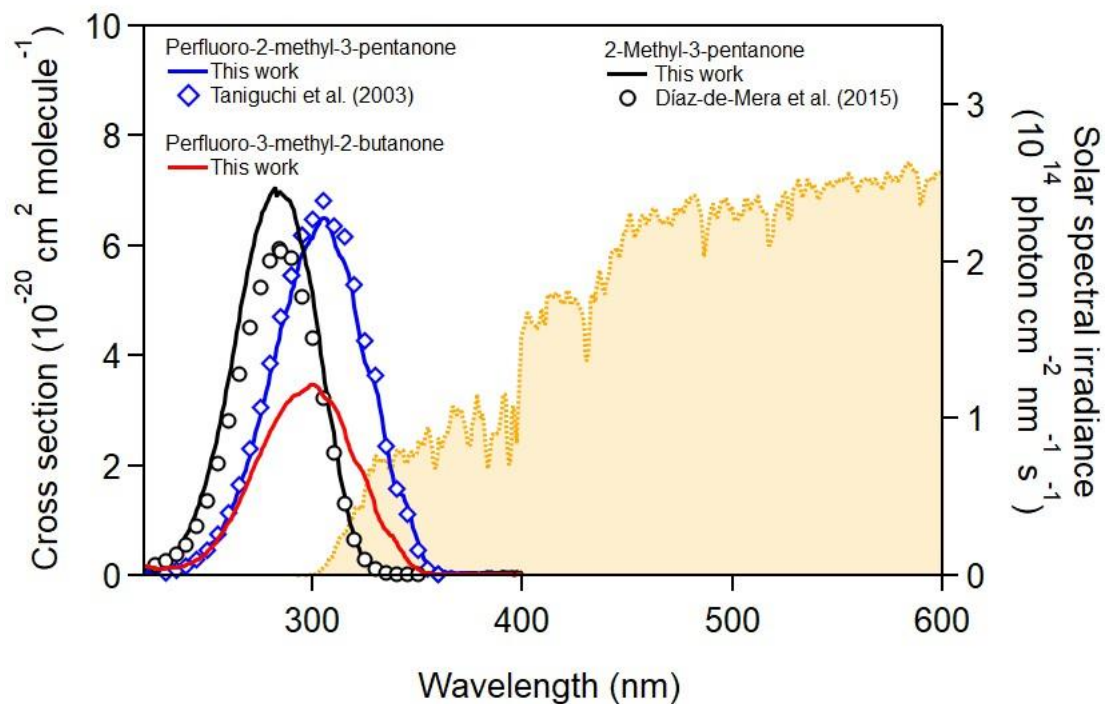
708 **Table 2.** Photolysis rate of perfluoro-2-methyl-3-pentanone (PF-2M3P), perfluoro-3-methyl-2-butanone (PF-3M2B) and 2-methyl-3-
 709 pentanone (2M3P) obtained in this work and compared to the reported data from the literature.
 710

Ketone	[Ketone] ₀ (10 ¹³ molecule cm ⁻³)	Chamber	Date	Irradiation	<i>J</i> (s ⁻¹)	<i>J</i> _{NO2} (s ⁻¹)	Atmospheric Lifetime (days)	Reference	
PF-2M3P	3.0-3.8	HELIOS	Sept 2013	Solar irradiation	(1.1-3.8)×10 ⁻⁶	(3.0-5.6)×10 ⁻³	3-11	This work	
	8.9-27	3.4 m ³ chamber	July 2010	Solar irradiation	(1.7-2.8) ×10 ⁻⁶	(4.4-5.5)×10 ⁻³	4-7	This work	
	8-64	Toledo, Spain	June-July 2013/2014	Solar irradiation	(6.8±0.8)×10 ⁻⁶		5.5±1.9	Díaz-de-Mera, et al. ¹³	
	2.5	Euphore	July 2003	Solar irradiation	(6.4±0.3)×10 ⁻⁶	7.85×10 ⁻³	~7	D'Anna, et al. ¹⁸	
	(0.55-6.5)×10 ³	140-L Pyrex reactor			14 blacklamps	(1.0±0.1)×10 ⁻⁷		7-14	Taniguchi, et al. ⁵
		47° N and 1° E ^a		a	TUV model	(0.4-2.8)×10 ⁻⁶			This work
		39.9° N and 4° W ^a		a	TUV model	(2.1±0.8)×10 ⁻⁶		5.5±1.9	Díaz-de-Mera, et al. ¹³
2M3P	Different latitude ^a		a	TUV model	(0.82-3.1)×10 ⁻⁶		4-14	Jackson, et al. ⁶	
PF-3M2B	3.0-3.4	HELIOS	Oct 2013	Solar irradiation	≤(2.6±1.4)×10 ⁻⁶	(2.2-5.6)×10 ⁻³	1-2	This work	
	47° N and 1° E ^a		a	TUV model	(0.3-2.8)×10 ⁻⁶			This work	
PF-3M2B	3.0-3.4	HELIOS	July 2017	Solar irradiation	(9±5)×10 ⁻⁷	(4.2-7.7)×10 ⁻³	~13	This work	
	47° N and 1° E ^a		a	TUV model	(0.2-1.2)×10 ⁻⁶			This work	

711 ^a yearly average;

712

713



714

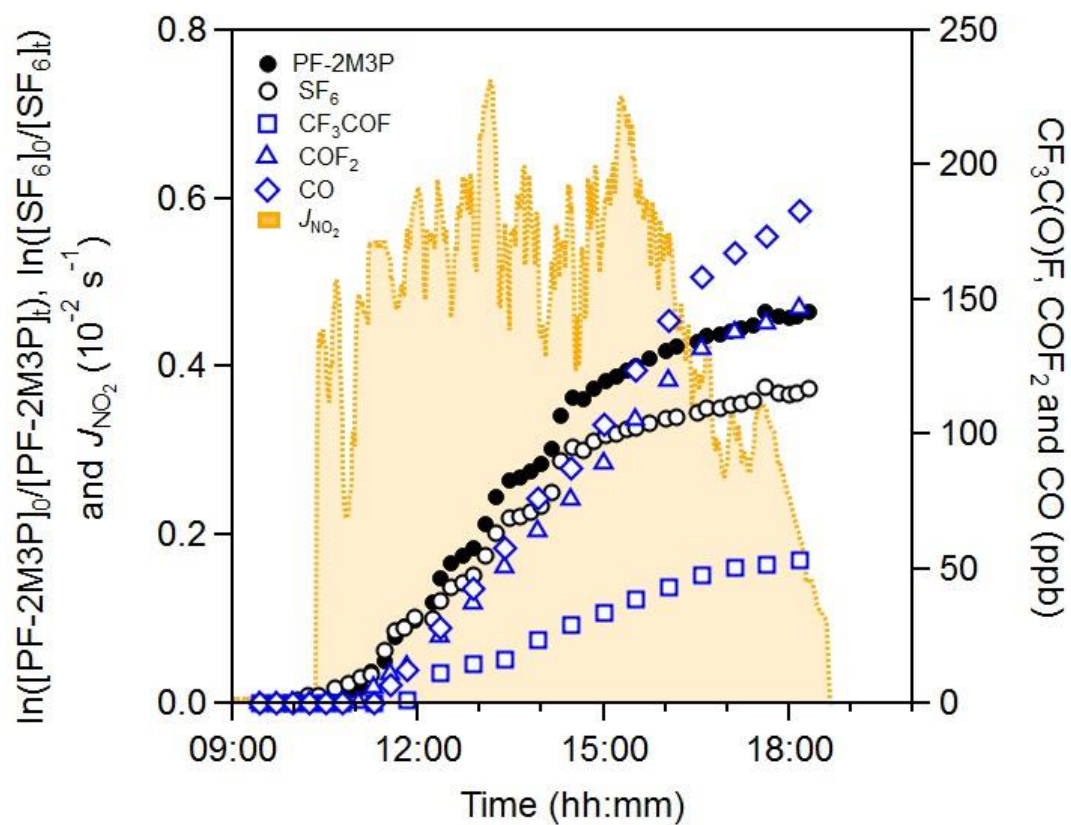
715

716

717 **Figure 1.** UV absorption spectra of perfluoro-2-methyl-3-pentanone (PF-2M3P),
718 perfluoro-3-methyl-2-butanone (PF-3M2B) and 2-methyl-3-pentanone (2M3P) and
719 compared with those from literature. The shaded area in yellow represents the solar
720 spectral irradiance measured inside HELIOS (13:00 local time, 27 September 2013).

721

722 *The figure 1 has been replaced*



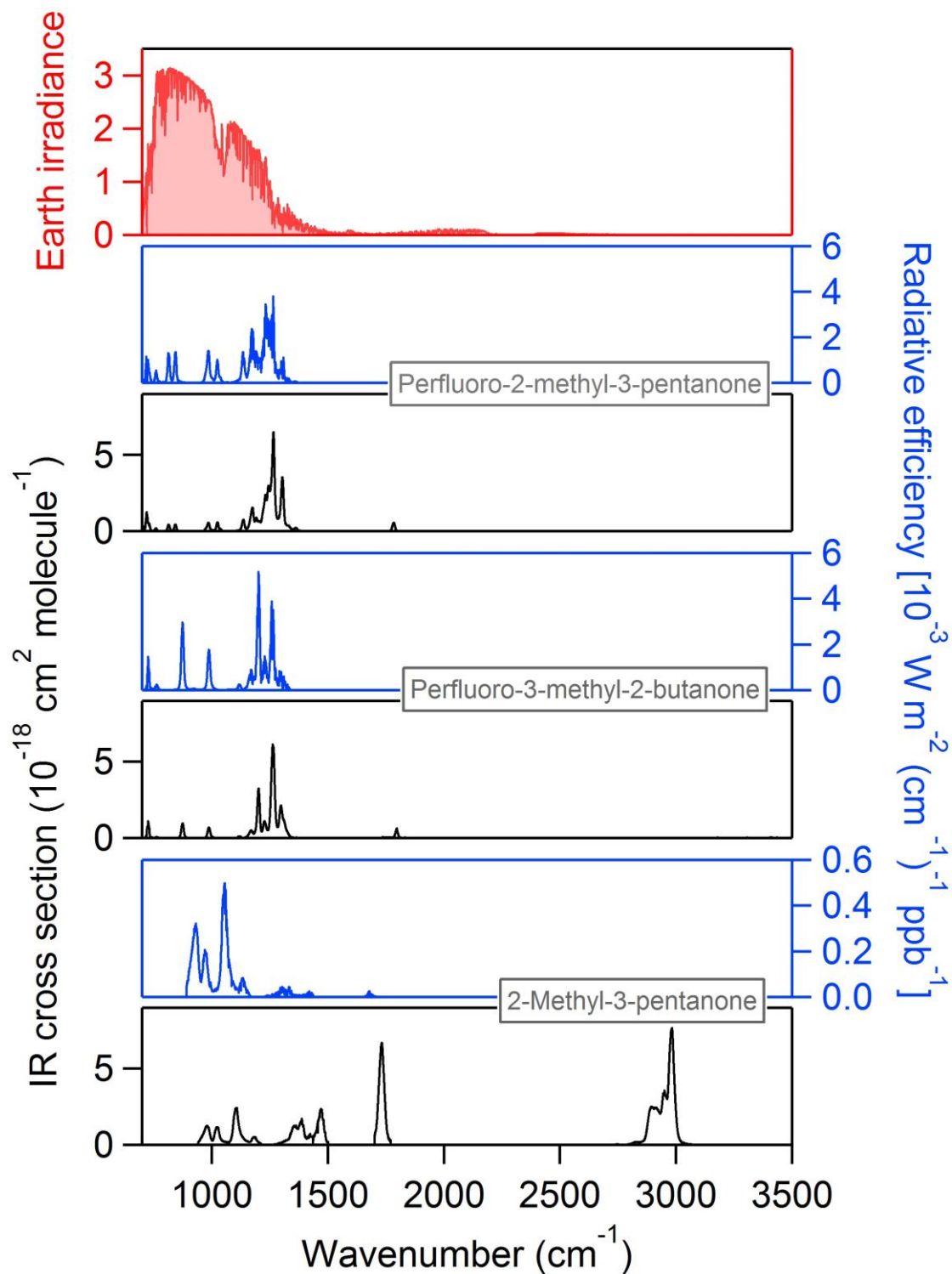
724

725

726

727

Figure 2. Perfluoro-2-methyl-3-pentanone (PF-2M3P) and its products during the photolysis experiment under natural irradiation in HELIOS (27 September 2013).



729
 730
 731
 732
 733
 734
 735
 736
 737
 738

Figure 3. Infrared absorption of perfluoro-2-methyl-3-pentanone, perfluoro-3-methyl-2-butanone and 2-methyl-3-pentanone and their contributions to the radiative efficiency. Earth's irradiance spectrum (top panel) is reported by Hodnebrog, et al.²⁵ (in units of $10^{-3} \text{ W m}^{-2} (\text{cm}^{-1})^{-1} \text{ ppb}^{-1}$ ($10^{-18} \text{ cm}^2 \text{ molecule}^{-1}$)⁻¹). The infrared absorption spectra measured in this work are showed in black, lower panel (in units of $10^{-18} \text{ cm}^2 \text{ molecule}^{-1}$, base e) and the radiative efficiency spectra are displayed in blue, upper panel (in units of $\text{W m}^{-2} (\text{cm}^{-1})^{-1} \text{ ppb}^{-1}$).